

# Influence of Gear Eccentricity with Non-Parallel Axis on the Dynamic Behaviour of a Gear Unit Using a Gear Slice Model with 26 Degrees of Freedom

Łukasz Jedliński<sup>1</sup>

<sup>1</sup> Faculty of Mechanical Engineering, Lublin University of Technology, Nadbystrzycka 36, 20-618, Lublin, Poland  
e-mail: l.jedlinski@pollub.pl

## ABSTRACT

This study investigates the problems of eccentricity and backlash using an analytical spur gear model with 26 degrees of freedom (DOF). Previous studies have only investigated the case of eccentricity with a parallel shift of the axis of rotation of the gear relative to its geometric axis of symmetry. This study presents a novel method for determining the radius of eccentricity and its angular position at any distance from the bearing support, in which the axis of rotation and the geometric axis of symmetry of the gear are non-parallel. The effect of gear motion in the line of action (LOA) and off-line of action (OLOA) directions on backlash is precisely determined, despite the fact that most studies usually ignore gear displacement along the OLOA direction. Numerical simulations are performed to determine the effect of eccentricity on backlash, and their results confirm that the proposed method for determining the radius of eccentricity for any eccentricity type is correct. A gear slice model is used for dynamic analysis. Results show that the type of eccentricity has a significant effect on the gear dynamics and that eccentricity analyses have to include other cases than merely eccentricity with parallel axes of gears.

**Keywords:** eccentricity, analytical model, backlash, slice coupling, spur gear.

## INTRODUCTION

Research on gears has been carried out for many years, and today one can observe a growing number of research publications on the subject. There are two main reasons why the subject of gears is generating so much interest among researchers. First, gears are used in many industries and are indispensable in applications requiring high reliability, efficiency and durability. In addition, they have compact design and dimensions, and their ranges of transmitted torque and gear ratios meet the requirements of most applications. Second, the interest in gears stems from new analytical capabilities resulting from the advances in science and computer performance as well as the development of computer programs.

The operation of gears is simulated through analytical models, numerical models or hybrid models in which some part of the model is analytical

and some numerical (e.g. finite element method). The main advantage of analytical models is affordable calculation time while that of numerical models is the possibility of obtaining accurate results by including many phenomena in the model. Since the problems raised in this paper are related to an analytical model, further considerations will focus on analytical modelling of gears.

Models of gears are usually created to solve a specific problem. The main research directions in this area include the determination of the effect of machining parameters on tooth profile [1–3], modelling of gear mesh stiffness [4–6], determination of the effect of manufacturing [7–9] and operational factors [10,11] on the dynamics, service life [12] and efficiency of gears [13].

The main problem raised in this paper is gear eccentricity. In addition to that, the effect of backlash is investigated. This effect is not always taken into account in gear models [9,14].

The basic model of backlash is expressed through a piece-wise linear function consisting of three intervals [15,16]. The first and third linear functions are used when the relative displacement of gears is higher than the backlash. Their slope value is usually equal to 1. The second function represents the relative position of the gears when the surfaces of the teeth are not in contact. Two approaches are adopted in this case. Either is the function equal to zero [17] or it is a linear function [18] with the slope of a straight line usually below 0.3 [15]. The zero value is more true to the real conditions of teeth meshing, while the approximation by the linear function with a small slope value allows faster and more accurate numerical calculations. The presented backlash model is modified in order to enable more accurate representation of the interaction between the teeth in mesh. The transition between the linear functions has the form of a corner. Li et al. [4] modified this shape and made it more gentle by introducing a curve in order to consider the effect of lubrication. The effect of backlash is often considered only in terms of mesh stiffness [4, 15, 16, 18, 19]. For a comprehensive analysis of backlash effect, mesh damping must also be considered. Yi et al. [20] investigated the effect of backlash on mesh damping in the same way as that for mesh stiffness by determining a derivative of time from position and total backlash. An asymmetric differential model of backlash with mesh stiffness and mesh damping was developed by Zuo et al. [21]. The backlash model for mesh stiffness used in this study was taken from that publication, but the backlash model was modified. The used models of backlash with mesh damping and mesh stiffness have rounded corners between the intervals, which ensures that numerical calculations will be accurate and that the presence of lubrication will be considered. The backlash value will be equal to zero when there is no contact between the teeth. There are few studies in which backlash is calculated in a very precise way. The backlash value is calculated precisely considering gear displacement in the LOA and OLOA directions. The displacement along the OLOA direction is usually either ignored or calculated in a simplified way. This affects the value of mesh stiffness. In addition, a modified equation of backlash with mesh damping is presented.

An important problem in dynamic analysis of gears is eccentricity. Eccentricity primarily results from the limited manufacturing accuracy of machinery components, while excessive eccentricity

results from manufacturing errors and operational factors such as bearing wear. Previous studies investigated eccentricity with a parallel-shifted axis of gear rotation relative to the geometric axis of symmetry [9, 22–25]. In terms of the centre of mass and the principal axis of inertia, this corresponds to a case of static unbalance. The effect of eccentricity on the mechanism of a clutch-helical two-stage gear was studied by Walha et al. [22]. The model had 27 DOF and the backlash was described by linear functions. The effect of tooth profile modification in a single-stage gear, considering eccentricity and relationship between backlash and mesh damping, was investigated using a dynamic model with 10 DOF in [23]. An analytical 16-DOF model of a single-stage gear considering eccentricity was validated experimentally by Zhao et al. [7]. There are currently no studies investigating the problem of eccentricity for a general case in which the axis of rotation and the geometric axis of symmetry of a gear are non-parallel. This case is very frequent in reality and corresponds to dynamic unbalance. A novel method was developed by the author for determining the radius of eccentricity at any distance from the bearing and its angular position, which makes it possible to analyse any type of eccentricity. An analysis of this case requires taking into account non-uniform contact of the teeth over the face width. To that end, a gear slice model is used. This model can be effectively used to investigate local defects of teeth [10,11], tooth profile modification [3,26] and assembly errors [27]. Gears were divided into 6 slices. An analytical model of a spur gear with 26 DOF was created. Different cases of eccentricity are analysed to demonstrate its effect on backlash value, and a numerical simulation is performed to determine the effect of eccentricity on selected parameters describing gear operation.

## **DETERMINATION OF SELECTED FACTORS AFFECTING THE FORCES ACTING ON MESHED TEETH AND GEAR SHAFTS**

### **Normal backlash in gears**

Backlash is required for the proper operation of gears, as it prevents teeth jamming and ensures proper lubrication and cooling. The presence of backlash affects gear dynamics and, more specifically, forces acting on the gear teeth. Sometimes,

there may be no contact between the teeth surfaces, which leads to a situation when the forces acting on the meshed teeth are equal to zero. In mathematical models, these forces are usually calculated based on the product of stiffness and relative displacement, as well as damping and relative velocity. To take the backlash into account, the displacement and relative velocity of the gears were modified through appropriate function relationships (1).

$$F_n = kx_{LOAB} + c\dot{x}_{LOAB} \quad (1)$$

where:  $kx_{LOAB}$  is the function of the relative displacement of the engaged teeth with backlash,

$\dot{x}_{LOAB}$  is the function of the relative velocity of the engaged teeth with backlash.

The function  $x_{LOAB}$  describing the relative displacement of the engaged teeth with backlash is based on studies [19,21]. It is expressed as:

$$x_{LOAB} = \frac{1}{\rho} \ln \frac{1 + e^{\rho m_r(x_k - b_r)}}{1 + e^{-\rho m_l(x_k - b_l)}} \quad (2)$$

where:  $\rho$  is the positive parameter softening the corners of the function (the higher the value, the sharper the corners),

$m_r, m_l$  is the slope, or the positive parameter describing the steepness of the line beyond the scope of backlash for the  $r$  – right and  $l$  – left side of the function,

$x_k$  is the relative position of the teeth in mesh without backlash along the LOA direction,

$b_r, b_l$  are the values of the half normal backlash on the left and the right side.

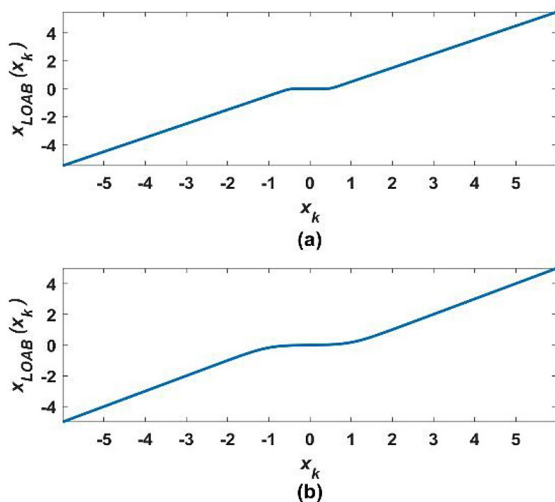


Fig. 1. Backlash function describing relative displacement of gears, for: (a)  $\rho = 20, b_r = b_l = 0.5$   
(b)  $\rho = 4, b_r = b_l = 1$

Figure 1 shows examples of plots obtained for the function  $x_{LOAB}$  for different values of the analysed parameters. In Figure 1a the total backlash value is 1, and in Figure 1b it equals 2.

If the presence of backlash is taken into account, a suitable function dependence must be used in calculations of viscous damping forces. The values of the viscous forces depend on the relative velocity of the gears. In a situation when the surfaces of the teeth are not in contact, the value of the function should be equal to zero, which will result in the value of the forces also being zero. For the teeth in mesh, the value of the relative velocity should not be changed, hence the value of the function should be either one or minus one. These assumptions are satisfied by the function developed based on [21]:

$$f_{vB} = \left| \frac{k_r e^{\rho m_r(x_k - b_r)}}{1 + e^{\rho m_r(x_k - b_r)}} \right| - \left| \frac{-k_l e^{\rho m_l(-x_k - b_l)}}{1 + e^{\rho m_l(-x_k - b_l)}} \right| \quad (3)$$

Examples of plots for the function are shown in Figure 2 for different values of the analysed parameters. In Figure 2a the total backlash value is 1, and in Figure 2b it is equal to 2.

The equation of function (3) can be used to determine the backlash value for the positive and the negative side individually. The sides are usually assigned the same values, as a result of which this function is odd, while the equation can be simplified to the form:

$$f_{vB} = \left| \frac{e^{\rho(x_k - b)}}{1 + e^{\rho(x_k - b)}} \right| - \left| \frac{e^{\rho(-x_k - b)}}{1 + e^{\rho(-x_k - b)}} \right| \quad (4)$$

The above relationship differs from the widely used ones [7, 28] in terms of a gentle

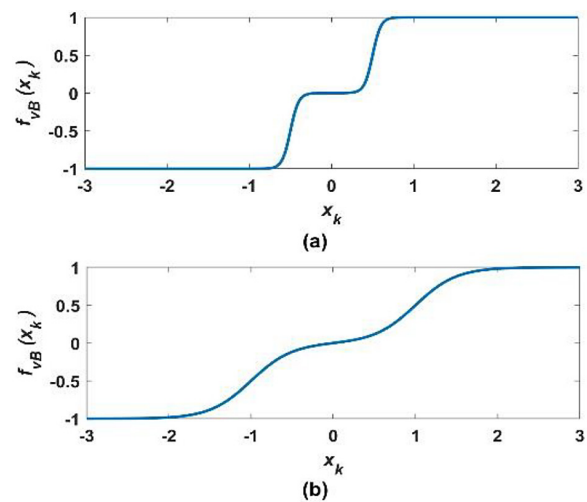


Fig. 2. Backlash function  $f_{vB}$  for calculating relative velocity of gears, for: (a)  $\rho = 20, b_r = b_l = 0.5$   
(b)  $\rho = 4, b_r = b_l = 1$

transition between the backlash zone and the tooth contact zone. The transition radius can freely be changed in a wide range in order to adjust it to the real conditions. This will ensure accuracy of numerical calculations. Backlash is frequently ignored in the calculation of damping forces [4, 15, 16, 18, 19]. For this case, it is necessary to use a different function than that used for calculating stiffness forces. The function  $f_{vB}$  makes it possible to determine values of half backlash, the slope transition between the values 0 and 1, as well as rounding radii.

### Eccentricity in gears

#### Eccentricity with parallel axes of gears relative to the theoretical axis of rotation

This is the simplest case for eccentricity analysis. It usually results from the fact that the gear is mounted eccentrically relative to the shaft, while their axes are parallel. This problem has been investigated in previous studies, e.g. in [9, 22–25]. None of these studies has, however, managed to precisely determine the effect of gear displacement along the OLOA direction on the distance between teeth surfaces along the LOA direction. This relationship was precisely described in [29]. This will serve as a basis for determining the displacement due to eccentricity, considering the effect of the displacement along the OLOA direction on the displacement of the meshed teeth along the LOA direction.

The displacement caused by eccentricity has impact on the relative position and velocity of the gear teeth and the centre distance. The change in the relative gear position along the LOA ( $x$ ) and OLOA ( $y$ ) axes is:

$$\begin{aligned} x_{pe} &= r_{pe} \cos(\varphi_p + \varphi_{pe}) \text{ is the LOA-axis direction,} \\ y_{pe} &= r_{pe} \sin(\varphi_p + \varphi_{pe}) \text{ is the OLOA-axis direction,} \\ x_{ge} &= r_{ge} \cos(\varphi_g + \varphi_{ge}) \text{ is the LOA-axis direction,} \\ y_{ge} &= r_{ge} \sin(\varphi_g + \varphi_{ge}) \text{ is the OLOA-axis direction,} \end{aligned}$$

where:  $p$  is the subscript denoting the pinion,  
 $g$  is the subscript denoting the gear,  
 $x_{pe}$  is the displacement caused by eccentricity along the  $x$  axis [m],  
 $y_{pe}$  is the displacement caused by eccentricity along the  $y$  axis [m],  
 $r_{pe}$  is the eccentricity radius [m].

The equations describing the relative displacement and velocity of the teeth with eccentricity are:

$$\begin{aligned} x_{LOA} &= r_{b1}\varphi_p + x_p - x_{py} + x_{pe} - \\ &\quad - r_{b2}\varphi_g + x_g - x_{gy} - x_{ge} \end{aligned} \quad (5)$$

$$\begin{aligned} \dot{x}_{LOA} &= r_{b1}\dot{\varphi}_p + \dot{x}_p - \dot{x}_{py} + \dot{x}_{pe} - \\ &\quad - r_{b2}\dot{\varphi}_g + \dot{x}_g - \dot{x}_{gy} - \dot{x}_{ge} \end{aligned} \quad (6)$$

The overall distance between the axes of the gears with eccentricity that is required for calculating  $x_{py}$  and  $x_{gy}$  is:

$$a_{w1} = |O_{11}O_2| = \sqrt{(a_w + f_p - f_g)^2 + (e_p - e_g)^2} \quad (7)$$

where:  $a_{w1} = |O_{11}O_2|$  is the centre distance of the gears with shifted profiles,

$O_2$  is the point of intersection with the axis of rotation of the gear,

$f_p = (y_p + y_{pe})\cos\alpha_w$  is the displacement of the axis of rotation of the pinion about the  $f$  axis,

$f_g = (y_g + y_{ge})\cos\alpha_w$  is displacement of the axis of rotation of the gear about the  $f$  axis,

$e_p = (y_p + y_{pe})\sin\alpha_w$  is the displacement of the axis of rotation of the pinion about the  $e$  axis,

$e_g = (y_g + y_{ge})\sin\alpha_w$  is the displacement of the axis of rotation of the gear about the  $e$  axis.

More information about the way of calculating the values of  $x_{py}$  and  $x_{gy}$  is given in [29].

#### Eccentricity with non-parallel axes of gears

This is a general case of gear eccentricity. In practice, this can occur under the following circumstances:

- eccentric mounting of the gear on the shaft, with non-parallel axes of the shaft and gear,
- eccentric mounting of the gear on the shaft, with parallel axes of the shaft and gear and non-parallel holes for shaft bearings,

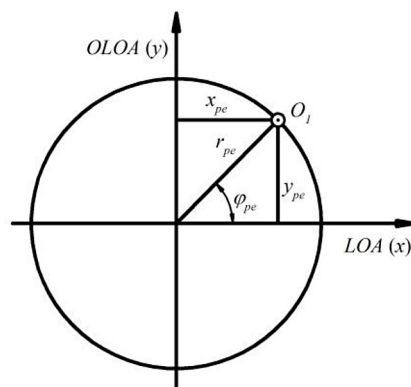


Fig. 3. Eccentricity of a pinion and its characteristic dimensions

Nomenclature	
$T_m, T_d$	input motor torque and output device torque
$I_m$	mass moment of inertia of the motor rotor and half of coupling
$I_p$	mass moment of inertia of the pinion, shaft and half of coupling (pinion subassembly)
$I_g$	mass moment of inertia of the gear, shaft and half of coupling (gear subassembly)
$I_d$	mass moment of inertia of the device rotor and half of coupling
$I_{px} (I_{py} = I_{py})$	mass moment of inertia of the pinion, shaft and half of coupling
$I_{gx} (I_{gy} = I_{gy})$	mass moment of inertia of the gear, shaft and half of coupling
$\ddot{\phi}$	angular acceleration: $\ddot{\phi}_m$ – motor rotor, $\ddot{\phi}_p$ – pinion, $\ddot{\phi}_g$ – gear, $\ddot{\phi}_d$ – device rotor
$\varphi_p, \varphi_g$	pinion and gear angular position
$\varphi_{pe}, \varphi_{ge}$	angular position of eccentricity of pinion and gear
$\varphi_{ps1}, \varphi_{gs1}$	angular position of the first slice of pinion and gear
$\ddot{\theta}_{px}, \ddot{\theta}_{gx}, \ddot{\theta}_{py}, \ddot{\theta}_{gy}$	angular acceleration of the pinion and gear
$\ddot{x}_p, \ddot{x}_g$	linear acceleration of the pinion and the gear
$x_{py}$	distance between new contact point and pinion tooth flank along LOA (x) caused by the movement of gears along OLOA (y)
$x_{gy}$	distance between new contact point and gear tooth flank along LOA (x) caused by the movement of gears along OLOA (y)
$x_{pe}, y_{pe}, x_{ge}, y_{ge}$	displacement caused by eccentricity of pinion and gear along the x axis and y axis
$x_{LOA}, \dot{x}_{LOA}$	relative displacement and velocity of the teeth
$\ddot{y}_p, \ddot{y}_g$	linear acceleration of the pinion and gear
$l_p, l_{pp}, l_{p(i)}$	distance between pinion's bearings, distance from bearing 1 to center of the mass of the pinion, distance from bearing 1 to the center of the mass of i-th slice of pinion
$l_g, l_{gg}, l_{g(i)}$	distance between gear's bearings, distance from bearing 3 to center of the mass of the gear, distance from bearing 3 to the center of the mass of i-th slice of gear
$r_{pe}, r_{ge}$	pinion and gear eccentricity radius
$r_{ps}, r_{gs}, r_m$	moment arm of force for the pinion slice, the gear slice, motor and device couplings
$F_n, F_f$	normal force, tooth friction force
$F_{kb1x}, F_{cb1x}$	reaction force of bearing from stiffness and damping (subscript 1, 2, 3, 4 – bearing 2, bearing 3, bearing 4)
$k_{b1}, c_{b1}$	stiffness and damping of bearing 1
Subscripts	
$p$	the pinion
$g$	the gear
$x$	the LOA-axis direction
$y$	the OLOA-axis direction
$e$	eccentricity
$b$	bearing
$k$	stiffness
$c$	damping

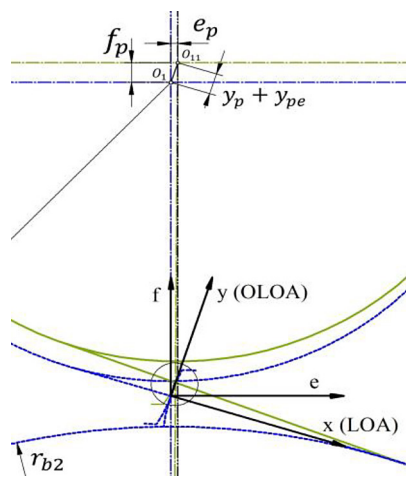


Fig. 4. Change in the centre distance of the pinion due to eccentricity and gear displacement along OLOA

- eccentricity caused by the bearings due to incorrect manufacturing, wear or operation (e.g. journal bearings).

As a result of non-parallel shaft axes, the meshing of the teeth occurs over a reduced face width and the location of the forces between the teeth varies. This affects the dynamic characteristics of gear operation.

Two cases of eccentricity with non-parallel axes of gears will be analysed. The first one is a special case and the other is a general case; however, the eccentricity will be considered for only one gear. It is assumed that the gear eccentricity is located at the bearing-mounted shaft, and this location is referred to as bearing eccentricity in a

later part of the manuscript. This means that the axis of the shaft and that of the gear overlap.

*Determination of eccentricity radius and angle of its location*

*Case 1*

This special case is easy to analyse, so the determination of eccentricity radius and angle will pose no problems. The real and theoretical axes of rotation of the shaft are non-parallel and they are located in one plane (Fig. 5). This occurs when the eccentricity values of the bearings differ while their eccentricity angles are the same.

The eccentricity radius for a given distance from bearing 1 is calculated using the equation

$$\varphi_l = \tan^{-1} \frac{r_{e2} - r_{e1}}{l} \quad (8)$$

$$c_{11} = (l - l_l) \tan \varphi_l \quad (9)$$

$$r_{el} = r_{e2} - c_{11} \quad (10)$$

where:  $r_{el}$  is the eccentricity radius being calculated,  $l_l$  is the distance from bearing 1 to the point where eccentricity is measured,  $l$  is the spacing between the bearings,  $r_{e1}, r_{e2}$  is the eccentricity of bearing 1 and bearing 2, respectively.

*Case 2*

The eccentricity radius  $r_{el}$  is determined in a plane that is perpendicular to the theoretical axis of rotation. For the general case, the real and

theoretical axes of the shaft are not in the same plane, as shown in Figure 6.

An additional distance of  $r_{min}$  is introduced, which is the minimum distance between the real and the theoretical axis. The value of  $r_{min}$  equals zero in Case 1 where the theoretical and real axes lie in one plane and are non-parallel (they intersect). The minimum distance has a special property. This property is characterized by the fact that the distance is always perpendicular to the theoretical and real axes. The sought eccentricity radius and other characteristic dimensions are shown in an orthogonal projection in Figure 7. The angle values were measured along the vertical axis

Calculations for determining the eccentricity radius  $r_{el}$  and its angle  $\varphi_{el}$  for a given distance  $l_l$  started with determining the distance  $l_{ex}$ :

$$l_{ex} = \sqrt{r_{e1}^2 + r_{e2}^2 - 2r_{e1}r_{e2}\cos(\varphi_{e1} - \varphi_{e2})} \quad (11)$$

In this equation, the  $\varphi_{e2}$  angle is subtracted from the  $\varphi_{e1}$  angle because it is assumed that the angles  $\varphi_{e1}$  and  $\varphi_{e2}$  measured counter-clockwise along the vertical axis have negative values.

An auxiliary angle is calculated:

$$\Delta r_{e2} l_{ex} = \sin^{-1} \left( \frac{r_{e1} \sin(\varphi_{e1} - \varphi_{e2})}{l_{ex}} \right) \quad (12)$$

together with the minimal distance between the axes:

$$r_{min} = r_{e2} \sin \Delta r_{e2} l_{ex} \quad (13)$$

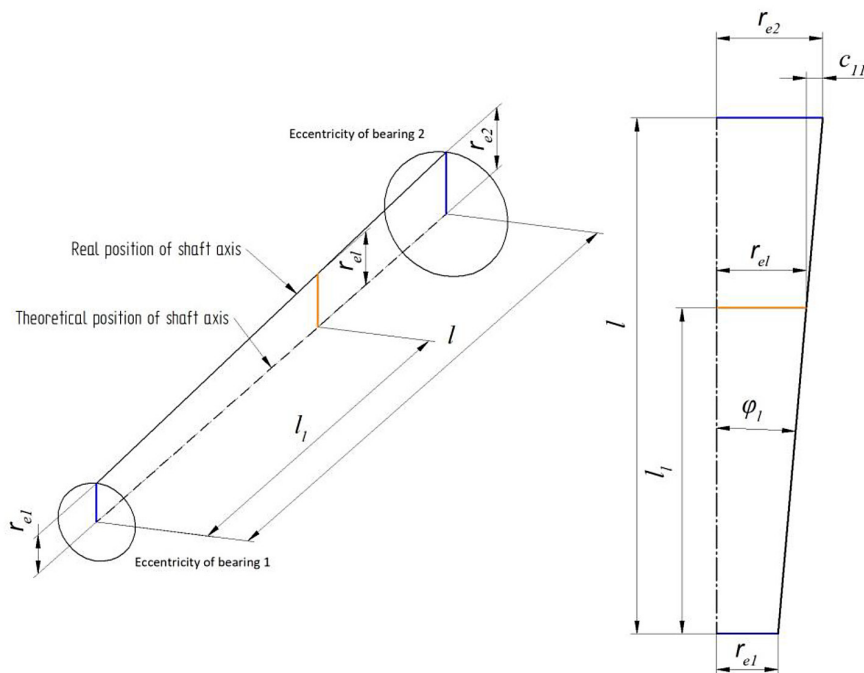


Fig. 5. Gear eccentricity for a special case

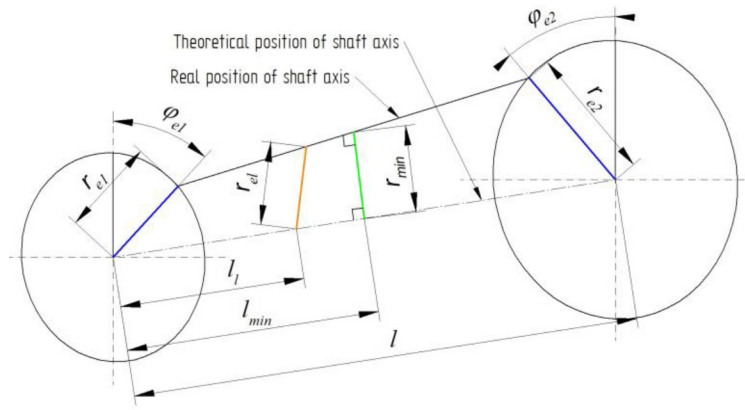


Fig. 6. Gear eccentricity for a general case

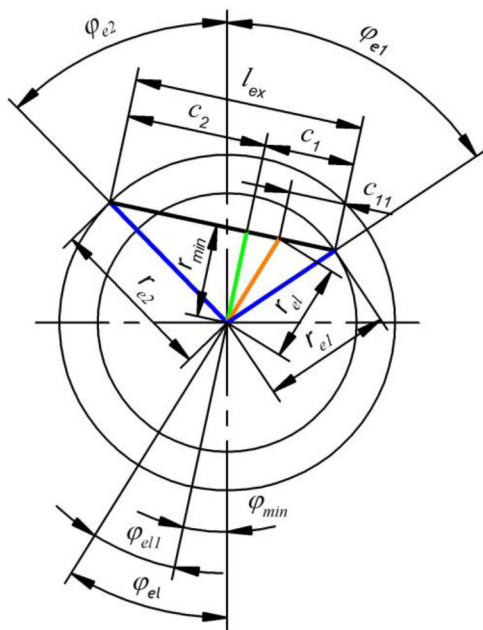


Fig. 7. Orthogonal projection of characteristic dimensions

and

$$\pm r_{min} r_{e2} = \cos^{-1} \left( \frac{r_{e1} \sin(\varphi_{e1} - \varphi_{e2})}{l_{ex}} \right) \quad (14)$$

hence the angle calculated along the vertical axis to the minimal distance is:

$$\varphi_{min} = \pm r_{min} r_{e2} + \varphi_{e2} \quad (15)$$

Other auxiliary quantities are calculated as:

$$c_1 = r_{e1} \sin(\varphi_{e1} - \varphi_{min}) \quad (16)$$

$$c_2 = r_{e2} \sin(\varphi_{e2} - \varphi_{min}) \quad (17)$$

The angle between the theoretical and real positions of the shaft axis (Fig. 8) is:

$$\varphi_l = \tan^{-1} \left( \frac{c_1 - c_2}{l} \right) \quad (18)$$

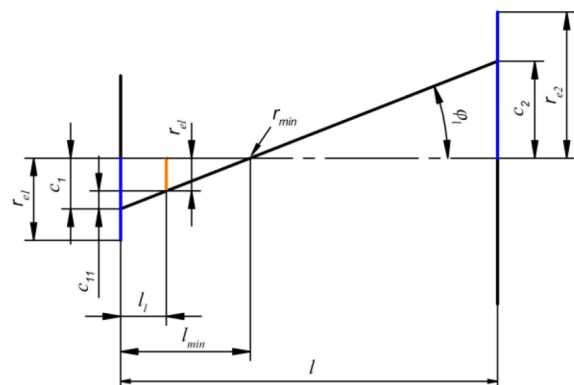


Fig. 8. Angle between the theoretical and real positions of a shaft axis

while the distance :

$$c_{11} = l_l \tan \varphi_l \quad (19)$$

The position of the minimal distance to bearing 1 is:

$$l_{min} = \frac{c_1}{\tan \varphi_l} \quad (20)$$

Finally, we can give equations describing the eccentricity radius  $r_{el}$  and eccentricity angle  $\varphi_{el}$  for a given distance  $l_l$  to bearing 1:

$$r_{el} = \sqrt{r_{min}^2 + (c_1 - c_{11})^2} \quad (21)$$

$$\varphi_{el} = \cos^{-1} \left( \frac{r_{min}}{r_{el}} \right) \quad (22)$$

The above derivation of the equations assumed that  $r_{e1} \leq r_{e2}$ . Equations describing relationships between the eccentricity radius and the eccentricity angle for the other cases can be derived in the same way, for all combinations of values of  $r_{e1}$ ,  $r_{e2}$ ,  $\varphi_{e1}$  and  $\varphi_{e2}$ .

### Forces occurring with shaft and gear eccentricity

#### Centrifugal force

Eccentricity is the source of centrifugal force and causes an increase in the load of shafts and bearings. In general, the centrifugal force for a pinion is:

$$F_{ep} = m_{pe} r_{pe} \omega_p^2 \quad (23)$$

and for a gear:

$$F_{eg} = m_{ge} r_{ge} \omega_g^2 \quad (24)$$

where:  $m_{pe}$  is the mass of a pinion that is eccentric,  $m_{ge}$  is the mass of a gear that is eccentric.

The centrifugal force in the LOA direction is:

$$F_{epx} = m_{pe} r_{pe} \dot{\varphi}_p^2 \cos(\varphi_{pt} + \varphi_{pel}) \quad (25)$$

$$F_{egx} = m_{ge} r_{ge} \dot{\varphi}_g^2 \cos(\varphi_{gt} + \varphi_{gel}) \quad (26)$$

and in the OLOA direction:

$$F_{epy} = m_{pe} r_{pe} \dot{\varphi}_p^2 \sin(\varphi_{pt} + \varphi_{pel}) \quad (27)$$

$$F_{egy} = m_{ge} r_{ge} \dot{\varphi}_g^2 \sin(\varphi_{gt} + \varphi_{gel}) \quad (28)$$

In real structures, eccentricity can occur between gear and shaft, shaft and housing or both. In the first situation only the gear mass should be included, and in the second we should consider the mass of a gear, shaft and half of coupling.

### ANALYSIS OF THE INFLUENCE OF ECCENTRICITY ON NORMAL BACKLASH

#### Normal backlash and eccentricity with parallel axes of gears

When backlash is included in the model, its value depends on eccentricity. By definition, the backlash is measured along the LOA direction.

To simplify the calculations, the displacement caused by eccentricity with parallel axes of the gears will be analysed for two characteristic directions: LOA and OLOA. The displacement along the LOA direction directly causes a 1 to 1 change in the normal backlash. Figure 9a shows the plot illustrating the relationship  $j_n = x_{pe}$ . A more complicated situation occurs when the displacement is along the OLOA direction. The value of the normal backlash changes as shown by the plot in Figure 9b. The backlash value is  $j_n = x_{pgy}$ . The last plot in Figure 9c shows the changes in normal backlash due to eccentricity for the displacement only along the LOA direction and that along the LOA and OLOA directions.

When the effect of eccentricity along the OLOA direction is taken into account, this always results in increased backlash.

#### Normal backlash and eccentricity with non-parallel axes of gears

In this section an analysis will be carried out for a general case of eccentricity, in which the gear axes are non-parallel. The cylindrical spur gear analysed for this case is characterized by the following parameters:  $m = 3$  mm,  $\alpha = 20^\circ$ ,  $z_1 = 30$ ,  $z_2 = 30$ . Other characteristic dimensions included a bearing spacing of  $l = 300$  mm and a face width of 60 mm. The eccentricity was located at the bearing mounting of the pinion and was denoted by  $r_{e1}$  (eccentricity of bearing 1) and  $r_{e2}$  (eccentricity of bearing 2). The angular position of bearing eccentricity was denoted by  $\varphi_{e1}$  and  $\varphi_{e2}$ . In the analysis, only the eccentric bearing mounting of the pinion shaft was considered, the axis of rotation of the second gear overlapped with the theoretical axis of rotation. The normal backlash value was calculated for one rotation of the pinion.

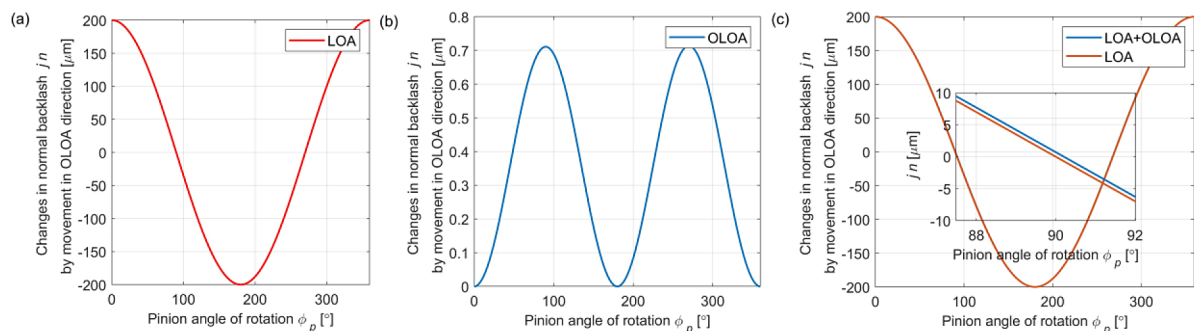


**Fig. 9.** Plots illustrating changes in normal backlash caused by pinion eccentricity  $r_{pe}$  during one revolution: (a) LOA – displacement only along LOA vs. normal backlash  $j_n = x_{pe}$ , (b) OLOA – displacement only along OLOA vs. normal backlash  $j_n = x_{pgy}$ , (c) LOA+OLOA – displacement along LOA and OLOA vs. normal backlash  $j_n = x_{pe} + x_{pgy}$

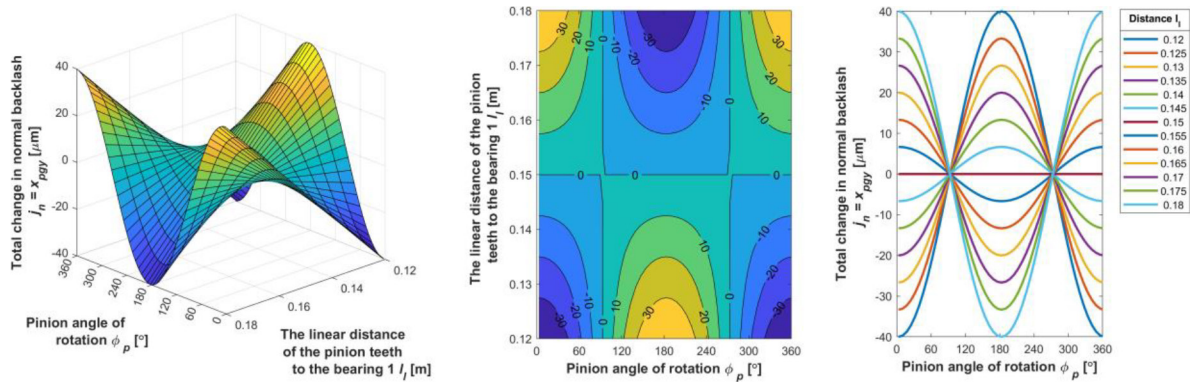


**Fig. 10.** Normal backlash  $j_n$  as a function of the pinion angle of rotation  $\phi_p$  and the linear distance  $l_l$  between pinion teeth and bearing 1, for:  $r_{e1} = r_{e2} = 200 \mu\text{m}$ ,  $\phi_{e1} = 180^\circ$  and  $\phi_{e2} = 0^\circ$ ,  $l_l = 0.12\text{--}0.18 \text{ m}$ ,  $l = 0.3 \text{ m}$

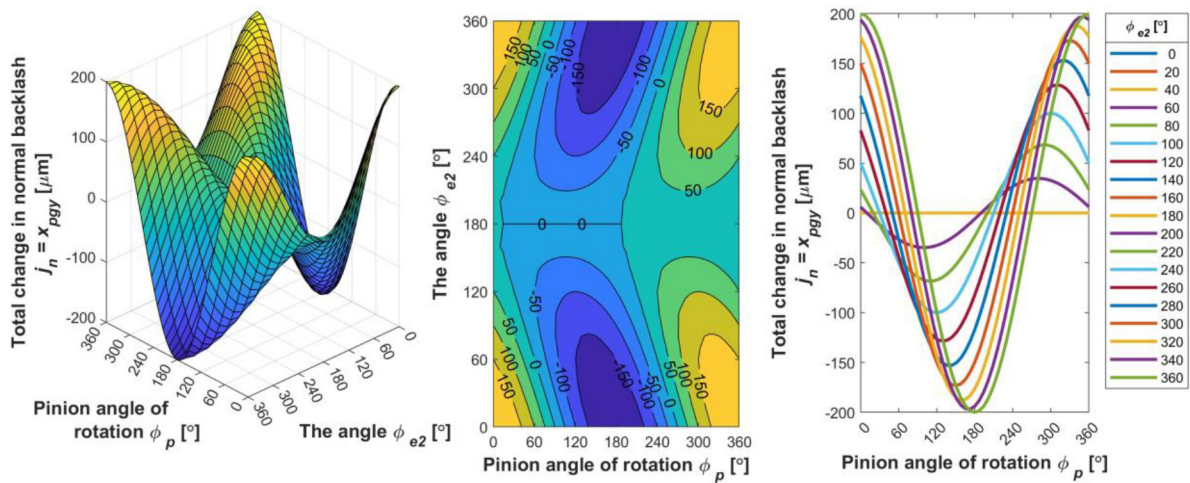


**Fig. 11.** Normal backlash  $j_n$  as a function of the pinion angle of rotation  $\phi_p$  and the eccentricity angle  $\phi_{e2}$  in bearing 2, for:  $r_{e1} = r_{e2} = 200 \mu\text{m}$ ,  $\phi_{e1} = 0^\circ$  and  $\phi_{e2} = 0\text{--}360^\circ$ ,  $l_l = 0.15 \text{ m}$ ,  $l = 0.3 \text{ m}$

The results in Figure 10 show the pinion eccentricity for the same eccentricity radii in the counter-phase  $\phi_{e1} = 180^\circ$  and  $\phi_{e2} = 0^\circ$ . The distance  $l_l$  to bearing 1 is changed, which is tantamount to testing the gear over the face width. For these parameters, the theoretical and real axes of rotation intersect in the middle of the distance between the bearings for  $l_l = 0.15 \text{ m}$ , which is reflected as the backlash value  $j_n = 0 \mu\text{m}$ . By increasing the distance from the point of intersection of the axes, the variations in the backlash value increase up to  $j_n = \pm 40 \mu\text{m}$ .

From the above analyses of the effect of eccentricity it follows that the normal backlash value depends on many parameters (Fig. 11). For the same value of bearing eccentricity  $r_{e1} = r_{e2} = 200 \mu\text{m}$ , the normal backlash value can range from  $0 \mu\text{m}$  to  $200 \mu\text{m}$ . For eccentricities with non-parallel axes, there are significant differences in backlash values obtained for the same gear depending on the location of eccentricity over the face width  $l_l$  (Fig. 10). The

relationships between eccentricity and normal backlash are nonlinear.

### 6-slice model of a spur gear unit

The standard analytical models of gears can only take into account the effect of eccentricity for parallel gear axes. For a more accurate representation of eccentricity effects, individual gear fragments must be considered independently. To that end, an analytical model of a gear unit was created, in which the face width was divided into slices. Each slice had an independent degree of freedom connected with rotation about the axis. Six slices were extracted for the pinion and gear. The connections between the slices were represented by stiffness and damping. The shafts were mounted in bearings and each support was allowed to move in two directions. Taking into account the couplings, the analytical model of a single-stage spur gear shown in Figure 12 had 26 DOF.

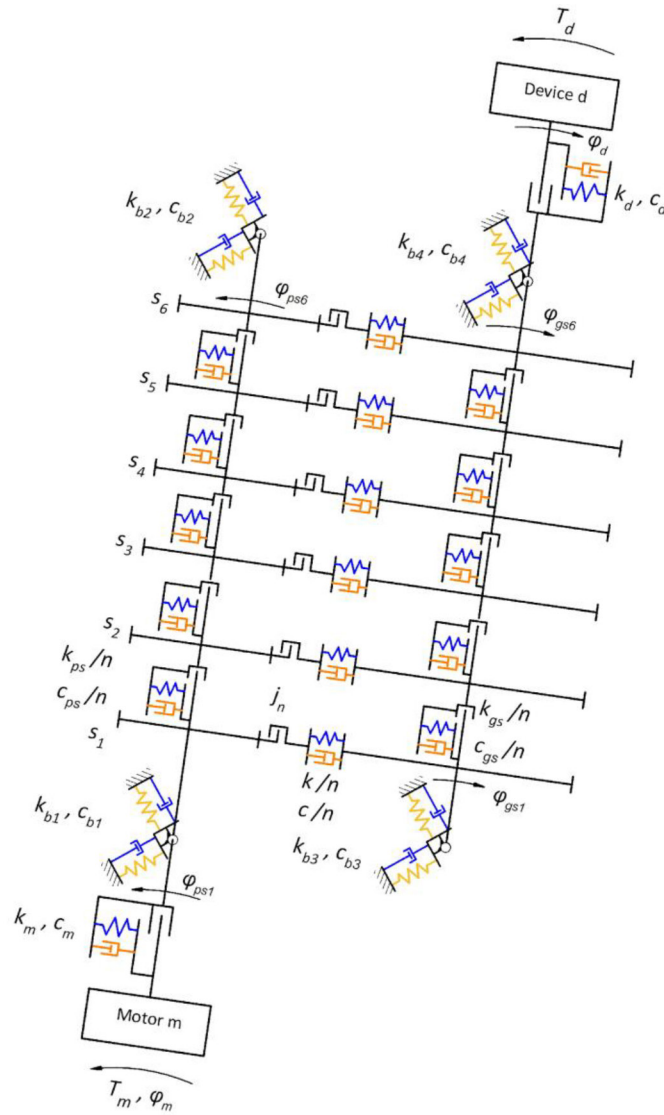


Fig. 12. Analytical model of a spur gear unit as divided into 6 slices, from  $s_1$  to  $s_6$

Equations of motion – rotation:

$$I_m \ddot{\phi}_m + M_{km} + M_{cm} = T_m \tag{29}$$

$$I_{ps1} \ddot{\phi}_{ps1} + M_{kp1} + M_{cp1} + M_{kps1} + M_{cps1} = M_{km} + M_{cm} + M_{fp1} \tag{30}$$

$$I_{ps2} \ddot{\phi}_{ps2} + M_{kp2} + M_{cp2} + M_{kps2} + M_{cps2} = M_{kps1} + M_{cps1} + M_{fp2} \tag{31}$$

$$I_{ps3} \ddot{\phi}_{ps3} + M_{kp3} + M_{cp3} + M_{kps3} + M_{cps3} = M_{kps2} + M_{cps2} + M_{fp3} \tag{32}$$

$$I_{ps4} \ddot{\phi}_{ps4} + M_{kp4} + M_{cp4} + M_{kps4} + M_{cps4} = M_{kps3} + M_{cps3} + M_{fp4} \tag{33}$$

$$I_{ps5} \ddot{\phi}_{ps5} + M_{kp5} + M_{cp5} + M_{kps5} + M_{cps5} = M_{kps4} + M_{cps4} + M_{fp5} \tag{34}$$

$$I_{ps6} \ddot{\phi}_{ps6} + M_{kp6} + M_{cp6} = M_{kps5} + M_{cps5} + M_{fp6} \tag{35}$$

$$I_{gs1} \ddot{\phi}_{gs1} + M_{kgs1} + M_{cgs1} + M_{fg1} = M_{kg1} + M_{cg1} \tag{36}$$

$$I_{gs2} \ddot{\phi}_{gs2} + M_{kgs2} + M_{cgs2} + M_{fg2} = M_{kg2} + M_{cg2} + M_{kgs1} + M_{cgs1} \tag{37}$$

$$I_{gs3} \ddot{\phi}_{gs3} + M_{kgs3} + M_{cgs3} + M_{fg3} = M_{kg3} + M_{cg3} + M_{kgs2} + M_{cgs2} \tag{38}$$

$$I_{gs4} \ddot{\phi}_{gs4} + M_{kgs4} + M_{cgs4} + M_{fg4} = M_{kg4} + M_{cg4} + M_{kgs3} + M_{cgs3} \tag{39}$$

$$I_{gs5}\ddot{\phi}_{gs5} + M_{kgs5} + M_{cgs5} + M_{fg5} = M_{kg5} + M_{cg5} + M_{kgs4} + M_{cgs4} \quad (40)$$

$$I_{gs6}\ddot{\phi}_{gs6} + M_{kgs6} + M_{cgs6} + M_{fg6} = M_{kg6} + M_{cg6} + M_{kgs5} + M_{cgs5} \quad (41)$$

$$I_d\ddot{\phi}_d + T_d = M_{kd} + M_{cd} \quad (42)$$

Equations of motion – plane motion parallel to LOA:

$$F_{kb1x}l_p + F_{cb1x}l_p + m_p\ddot{x}_{pCOM}(l_p - l_{pp}) - I_{px}\ddot{\theta}_{px} - M_{pGyrx} = -M_{pCx1} + M_{pNx1} \quad (43)$$

$$F_{kb2x}l_p + F_{cb2x}l_p + m_p\ddot{x}_{pCOM}l_{pp} + I_{px}\ddot{\theta}_{px} + M_{pGyrx} = -M_{pCx2} + M_{pNx2} \quad (44)$$

$$F_{kb3x}l_g + F_{cb3x}l_g + m_g\ddot{x}_{gCOM}(l_g - l_{gg}) + I_{gx}\ddot{\theta}_{gx} - M_{gGyrx} = M_{gCx3} + M_{gNx3} \quad (45)$$

$$F_{kb4x}l_g + F_{cb4x}l_g + m_g\ddot{x}_{gCOM}l_{gg} - I_{gx}\ddot{\theta}_{gx} + M_{gGyrx} = M_{gCx4} + M_{gNx4} \quad (46)$$

Equations of motion – plane motion parallel to OLOA:

$$F_{kb1y}l_p + F_{cb1y}l_p + m_p\ddot{y}_{pCOM}(l_p - l_{pp}) - I_{py}\ddot{\theta}_{py} + M_{pGyry} = -M_{pCy1} + M_{pfy1} \quad (47)$$

$$F_{kb2y}l_p + F_{cb2y}l_p + m_p\ddot{y}_{pCOM}l_{pp} + I_{py}\ddot{\theta}_{py} - M_{pGyry} = -M_{pCy2} + M_{pfy2} \quad (48)$$

$$F_{kb3y}l_g + F_{cb3y}l_g + m_g\ddot{y}_{gCOM}(l_g - l_{gg}) + I_{gy}\ddot{\theta}_{gy} + M_{gGyry} = -M_{gCy3} + M_{gfy3} \quad (49)$$

$$F_{kb4y}l_g + F_{cb4y}l_g + m_g\ddot{y}_{gCOM}l_{gg} - I_{gy}\ddot{\theta}_{gy} - M_{gGyry} = -M_{gCy4} + M_{gfy4} \quad (50)$$

$M_{km} = k_m(\phi_m - \phi_{ps1})r_m$  is the moment due to coupling stiffness,

$M_{cm} = c_m(\dot{\phi}_m - \dot{\phi}_{ps1})r_m$  is the moment due to coupling damping,

$M_{kp1} = \frac{k}{n}r_{b1}[r_{b1}\phi_{ps1} + x_{p1} - x_{p1y} + x_{pe1} - r_{b2}\phi_{gs1} + x_{g1} - x_{g1y} + x_{ge1}]$  is the moment due to the stiffness of slice 1 of pinion and gear acting on the pinion,

$n$  – number of gear slices,

$M_{cp1} = \frac{c}{n}r_{b1}[r_{b1}\dot{\phi}_{ps1} + \dot{x}_{p1} - \dot{x}_{p1y} + \dot{x}_{pe1} - r_{b2}\dot{\phi}_{gs1} + \dot{x}_{g1} - \dot{x}_{g1y} + \dot{x}_{ge1}]$  is the moment due to the damping of slice 1 of pinion and gear acting on the pinion,

$x_{p1} = x_{b1} + l_{p1}\frac{x_{b2}-x_{b1}}{l_p}$  is the displacement of the centre of pinion slice 1 due to shaft displacements in the bearings along the LOA direction,

$x_{p1y}$  is the displacement of the centre of pinion slice 1 due to eccentricity and shaft displacements in the bearings along the OLOA direction, calculated according to [29],

$x_{pe1} = r_{ep1}\cos(\phi_{ps1} + \phi_{pe1})$  is the displacement of the centre of pinion slice 1 due to eccentricity,

$M_{kg1} = \frac{k}{n}r_{b2}[r_{b1}\phi_{ps1} + x_{p1} - x_{p1y} + x_{pe1} - r_{b2}\phi_{gs1} + x_{g1} - x_{g1y} + x_{ge1}]$  is the moment due to the stiffness of slice 1 of pinion and gear acting on the gear,

$M_{cg1} = \frac{c}{n}r_{b2}[r_{b1}\dot{\phi}_{ps1} + \dot{x}_{p1} - \dot{x}_{p1y} + \dot{x}_{pe1} - r_{b2}\dot{\phi}_{gs1} + \dot{x}_{g1} - \dot{x}_{g1y} + \dot{x}_{ge1}]$  is the moment due to the damping of slice 1 of pinion and gear acting on the gear,

$x_{g1} = x_{b4} + (l_g - l_{g1})\frac{x_{b3}-x_{b4}}{l_g}$  is the displacement of the centre of gear slice 1 due to shaft displacements in the bearings along the LOA direction,

$x_{g1y}$  is the displacement of the centre of gear slice 1 due to eccentricity and shaft displacements in the bearings along the OLOA direction, calculated according to [29],

$x_{ge1} = r_{eg1} \cos(\varphi_{gs1} + \varphi_{ge1})$  is the displacement of the centre of gear slice 1 due to eccentricity,

$M_{kps1} = \frac{k_{ps}}{n} (\varphi_{ps1} - \varphi_{ps2}) r_{ps}$  is the moment due to stiffness between pinion slices,

$M_{cps1} = \frac{c_{ps}}{n} (\dot{\varphi}_{ps1} - \dot{\varphi}_{ps2}) r_{ps}$  is the moment due to damping between pinion slices,

$M_{kgs1} = \frac{k_{gs}}{n} (\varphi_{gs1} - \varphi_{gs2}) r_{gs}$  is the moment due to stiffness between pinion slices,

$M_{cgs1} = \frac{c_{gs}}{n} (\dot{\varphi}_{gs1} - \dot{\varphi}_{gs2}) r_{gs}$  is the moment due to damping between pinion slices,

$M_{kd} = k_d (\varphi_{g6} - \varphi_d) r_m$  is the moment due to coupling stiffness,

$M_{cd} = c_d (\dot{\varphi}_{g6} - \dot{\varphi}_d) r_m$  is the moment due to coupling damping,

$M_{pGx} = I_p \dot{\varphi}_{p1} \dot{\theta}_{py}$  is the gyrostatic moment acting on the pinion in plane parallel to LOA,

$M_{pCx1} = \sum_{i=1}^n m_{ps(i)} r_{pe(i)} \dot{\varphi}_{ps(i)}^2 \cos(\varphi_{ps(i)} + \varphi_{pe(i)}) (l_p - l_{p(i)})$  is the centrifugal moment of the pinion slices in plane parallel to LOA relative to bearing 1,

$M_{pNx1} = \sum_{i=1}^n F_{n(i)} (l_p - l_{p(i)})$  is the axial force acting on the pinion in plane parallel to LOA relative to bearing 1,

$M_{pfy1} = \sum_{i=1}^n F_{f(i)} (l_p - l_{p(i)})$  is the moment of friction of the pinion slices in plane parallel to OLOA relative to bearing 1.

## NUMERICAL RESULTS

This section investigates the effect of eccentricity on selected dynamic parameters of a gear unit. Specifically, the following are considered: backlash, friction, relationship between gear displacement along the OLOA direction and backlash, as well as dynamic transmission error (DTE). The stiffness of the teeth was described by the Cai model, which is discussed in detail in [30]. Eccentricity-induced changes were only implemented for the pinion. The applied parameters of the gears are listed in Table 1.

The first analysis involved determining the effect of backlash with pinion shaft eccentricity on DTE. The backlash was varied in the range from 50  $\mu\text{m}$  to 300  $\mu\text{m}$ . To establish a point of reference for DTE variation, calculations were made for a case when the backlash was equal to 0. The eccentricity parameters were  $r_{e1} = r_{e2} = 200 \mu\text{m}$ ,  $\varphi_{e1} = 0^\circ$  and  $\varphi_{e2} = 180^\circ$ , and the results are shown for the first gear slices described by  $l_i = 0.133$ .

In Figure 13 one can observe a clear change in DTE relative to the case then backlash was equal 0. The higher the signal value is, the lower

the value of DTE becomes. This means that a higher backlash value has a positive effect on decreasing the DTE value.

The aim of the second analysis was to examine the effect of eccentricity on all slices of the pinion. The eccentricity parameters applied in this analysis were the same as those used in the previous one, i.e.  $r_{e1} = r_{e2} = 200 \mu\text{m}$ ,  $\varphi_{e1} = 0^\circ$  and  $\varphi_{e2} = 180^\circ$ . These parameters show that the intersection between the real and the theoretical axis of rotation is the halfway distance

**Table 1.** Main parameters of gears

Parameter	Pinion	Gear
Number of teeth	$z_p = 30$	$z_g = 30$
Module [mm]	$m = 3$	
Pressure angle [°]	$\alpha_0 = 20$	
Face width [mm]	$B = 40$	
Torque [Nm]	$T = 31.8$	
Backlash [ $\mu\text{m}$ ]	$b = 40$	
Coefficient of teeth height y	1	
Top clearance coefficient $c^*$	0.25	
Sliding friction factor $\mu$	0.015	

between the bearings. The gears are located in the centre of the shafts. This means that the eccentricity radius is the lowest for the middle slices and the highest for the outer slices. Obtained results are plotted for three parameters: DET, torsional vibration acceleration of pinion slices and vibration acceleration of four bearings in plane parallel to LOA. Figure 14 reveals that the highest DTE value was obtained for outer slices 1 and 6 and the lowest for slices 3 and 4. The eccentricity radius has a decisive impact on DET. A different situation can be observed for torsional vibration acceleration (Fig. 15). Slices 1 through 4 exhibit similar vibration amplitudes. The highest values can be observed for the last pinion slices 5 and 6. This may result from the fact that slice 6 is only connected to slice 5, which decreases the torsional stiffness of these slices. The final plot (Fig. 16) in this analysis shows the vibration values obtained for four bearings. The values are similar, which indicates that the bearings were under a uniform load. This results from a symmetric change in the eccentricity radius of the slices relative to the centre of the gears

## CONCLUSIONS

This paper presented a novel method for analysing gear eccentricity for a general case in which the axis of rotation of the shaft and the geometric axis of symmetry of the gear were non-parallel. The study was conducted on a single-stage gear unit with cylindrical spur gears. A model consisting of six gear slices was created, in which the contact between the teeth would vary over the face width. The developed analytical model had a total of 26 DOF. In addition to that, the backlash with gear shafts moving in the LOA and OLOA directions was precisely determined. The backlash affected both mesh stiffness and mesh damping. Functions used for backlash representation were plotted. The backlash function responsible for damping was modified. Both functions showed smooth transitions between the parts responsible for the teeth position in backlash and in mesh. This provided a more accurate representation of the operation of lubricated gears.

The first analysis investigated the effect of eccentricity on backlash. The eccentricity occurred in the pinion bearings. It was changed

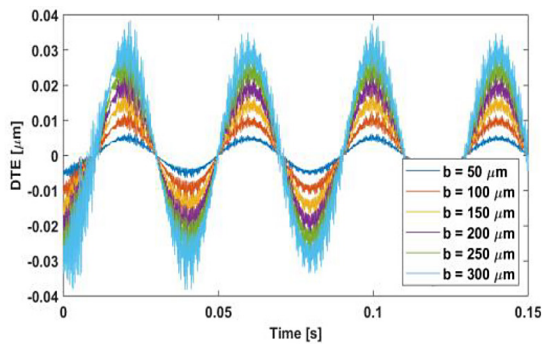


Fig. 13. Backlash  $b$  versus DTE

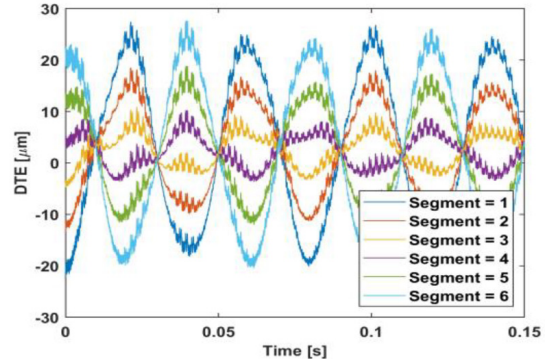


Fig. 14. DTE of gear slices

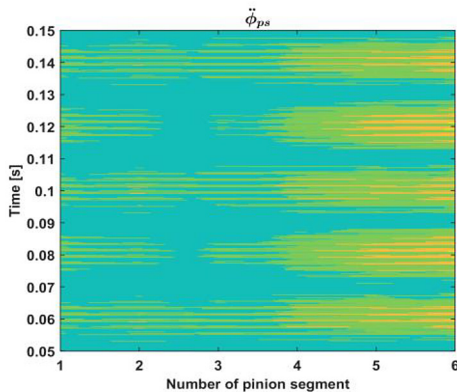


Fig. 15. Vibration of pinion slices

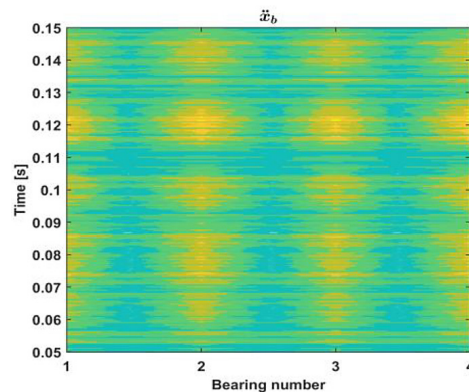


Fig. 16. Vibration of gear bearings

by varying the eccentricity radius value in the bearings and its position. The value of the backlash was determined for the centre of the shaft (gear) as well as for several positions at the same time. For the same ranges of eccentricity parameters, the backlash had different values, which showed that it was important not only to take eccentricity into account in the model, but also to implement the model with a suitable eccentricity case.

In the other analysis, the effects of two cases of eccentricity on DTE, torsional vibration of pinion slices and linear vibration of bearings were investigated, and the impact of backlash on DTE was determined. Summing up the results, it can be claimed that the eccentricity and backlash significantly affected the dynamics of gears. It was not enough to consider eccentricity for the case in which the axis of rotation of the shaft and the geometric axis of symmetry of the gear were parallel. This was a special case that is quite rare in real designs, and the change in eccentricity for the same eccentricity radius value of the bearing significantly affected the gear dynamics. The proposed method for determining the radius of eccentricity at any point of a gear only based on the value and position of eccentricity will contribute to more accurate dynamic analyses of gears. Implementation and calculations were made in Matlab and Simulink.

## REFERENCES

- Ding S, Chen Z, Zhang H, Yang W, Wu W, Song A. Gear evaluation deviations-based crucial geometric error identification of five-axis CNC gear form grinding process. 2023; 99: 663–675.
- Carranza Fernandez R, Tobie T, Rommel S, Collazo J. Improve wind gears bending performance by means of IGS (Improved gear surface). *Int J Fatigue*. 2023; 172: 107618.
- Sun Z, Chen S, Hu Z, Tao X. Improved mesh stiffness calculation model of comprehensive modification gears considering actual manufacturing. *Mech Mach Theory*. 2022; 167: 104470. <https://doi.org/10.1016/j.mechmachtheory.2021.104470>
- Li Z, Zhu C, Liu H, Gu Z. Mesh stiffness and nonlinear dynamic response of a spur gear pair considering tribo-dynamic effect: Manuscript submitted for publication in *Mechanism and Machine Theory*. *Mech Mach Theory*. 2020; 153: 103989. <https://doi.org/10.1016/j.mechmachtheory.2020.103989>
- Zhang C, Dong H, Wang D, Dong B. A new effective mesh stiffness calculation method with accurate contact deformation model for spur and helical gear pairs. *Mech Mach Theory*. 2022; 171: 104762. <https://doi.org/10.1016/j.mechmachtheory.2022.104762>
- Jordan JM, Blockmans B, Desmet W. A linear formulation for misaligned helical gear contact analysis using analytical contact stiffnesses. *Mech Mach Theory*. 2023; 187.
- Zhao Y, Liu Y, Xin X, Yu S, Ma H, Han Q. Dynamic Modelling Considering Nonlinear Factors of Coupled Spur Gear System and Its Experimental Research. *IEEE Access*. 2020; 8: 84971–8480.
- Mo S, Li Y, Wang D, Hu X, Bao H, Cen G, et al. An analytical method for the meshing characteristics of asymmetric helical gears with tooth modifications. *Mech Mach Theory*. 2023; 185: 1–17.
- Zhao B, Huangfu Y, Ma H, Zhao Z, Wang K. The influence of the geometric eccentricity on the dynamic behaviors of helical gear systems. *Eng Fail Anal*. 2020; 118: 104907. <https://doi.org/10.1016/j.engfailanal.2020.104907>
- Wu X, Luo Y, Li Q, Shi J. A new analytical model for evaluating the time-varying mesh stiffness of helical gears in healthy and spalling cases. *Eng Fail Anal*. 2022; 131: 105842. <https://doi.org/10.1016/j.engfailanal.2021.105842>
- Ning J, Chen Z, Wang Y, Li Y, Zhai W. Vibration feature of spur gear transmission with non-uniform depth distribution of tooth root crack along tooth width. *Eng Fail Anal*. 2021; 129: 105713. <https://doi.org/10.1016/j.engfailanal.2021.105713>
- Li Y, Wei P, Xiang G, Jia C, Liu H. Gear contact fatigue life prediction based on transfer learning. *Int J Fatigue*. 2023; 173.
- Hong I, Aneshansley E, Chaudhury K, Talbot D. Stochastic microcontact model for the prediction of gear mechanical power loss. *Tribol Int*. 2023; 183.
- Wang Y, Wang H, Li K, Qiao B, Shen Z, Chen X. An analytical method to calculate the time-varying mesh stiffness of spiral bevel gears with cracks. *Mech Mach Theory*. 2023; 188: 105399. <https://doi.org/10.1016/j.mechmachtheory.2023.105399>
- Kim TC, Rook TE, Singh R. Super- and sub-harmonic response calculations for a torsional system with clearance nonlinearity using the harmonic balance method. *J Sound Vib*. 2005; 281: 965–993.
- Moradi H, Salarieh H. Analysis of nonlinear oscillations in spur gear pairs with approximated modelling of backlash nonlinearity. *Mech Mach Theory*. 2012; 51: 14–31. <http://dx.doi.org/10.1016/j.mechmachtheory.2011.12.005>
- Akoto CL, Spangenberg H. Modeling of backlash in drivetrains. 4th CEAS Air Sp Conf. 2013.

18. Saghafi A, Farshidianfar A. An analytical study of controlling chaotic dynamics in a spur gear system. *Mech Mach Theory*. 2016; 96: 179–191.
19. Margielewicz J, Gaska D, Litak G. Modelling of the gear backlash. *Nonlinear Dyn*. 2019; 97: 355–368.
20. Xiong Y, Huang K, Xu F, Yi Y, Sang M, Zhai H. Research on the influence of backlash on mesh stiffness and the nonlinear dynamics of spur gears. *Appl Sci*. 2019; 9: 1–13.
21. Zuo Z, Ju X, Ding Z. Control of Gear Transmission Servo Systems with Asymmetric Deadzone Nonlinearity. *IEEE Trans Control Syst Technol*. 2016; 24: 1472–1479.
22. Walha L, Driss Y, Khabou MT, Fakhfakh T, Haddar M. Effects of eccentricity defect on the nonlinear dynamic behavior of the mechanism clutch-helical two stage gear. *Mech Mach Theory*. 2011; 46: 986–997.
23. Liu H, Zhang C, Xiang CL, Wang C. Tooth profile modification based on lateral- torsional-rocking coupled nonlinear dynamic model of gear system. *Mech Mach Theory*. 2016; 105: 606–619. <http://dx.doi.org/10.1016/j.mechmachtheory.2016.07.013>
24. Yu W, Mechefske CK, Timusk M. The dynamic coupling behaviour of a cylindrical geared rotor system subjected to gear eccentricities. *Mech Mach Theory*. 2017; 107: 105–122. <http://dx.doi.org/10.1016/j.mechmachtheory.2016.09.017>
25. He X, Zhou X, Xue Z, Hou Y, Liu Q, Wang R. Effects of gear eccentricity on time-varying mesh stiffness and dynamic behavior of a two-stage gear system. *J Mech Sci Technol*. 2019; 33: 1019–1032.
26. Chung WJ, Park JH, Yoo HG, Park YJ, Kim S chul, Sohn J hyeon, et al. Improved analytical model for calculating mesh stiffness and transmission error of helical gears considering trochoidal root profile. *Mech Mach Theory*. 2021; 163: 104386. <https://doi.org/10.1016/j.mechmachtheory.2021.104386>
27. He Z, Zhang T, Lin T. Novel mathematical modelling method for meshing impact of helical gear. *Mech Mach Theory*. 2020; 152.
28. Xiang L, Gao N. Coupled torsion–bending dynamic analysis of gear-rotor-bearing system with eccentricity fluctuation. *Appl Math Model*. 2017; 50: 569–584.
29. Jedliński Ł. Influence of the movement of involute profile gears along the off-line of action on the gear tooth position along the line of action direction. *Eksploat i Niezawodn*. 2021; 23: 736–744.
30. Jedlinski L. Analysis of the influence of gear tooth friction on dynamic force in a spur gear. *J Phys Conf Ser*. 2021; 1736.